A Statistical Study of the Solar Wind Turbulence at Ion Kinetic Scales Using the k-filtering Technique and Cluster Data

Roberts, Owen; Li, Xing; Jeska, Lauren

Published in:
Astrophysical Journal

DOI:
10.1088/0004-637X/802/1/2

Publication date:
2015

Citation for published version (APA):
Roberts, O., Li, X., & Jeska, L. (2015). A Statistical Study of the Solar Wind Turbulence at Ion Kinetic Scales Using the k-filtering Technique and Cluster Data. *Astrophysical Journal*, *802*(1), 1-13. https://doi.org/10.1088/0004-637X/802/1/2

The Astrophysical Journal, 802:2 (13pp), 2015 March 20 doi:10.1088/0004-637X/802/1/2

A STATISTICAL STUDY OF THE SOLAR WIND TURBULENCE AT ION KINETIC SCALES USING THE *K*-FILTERING TECHNIQUE AND CLUSTER DATA

O. W. Roberts, X. Li, and L. Jeska
Department of Physics, Aberystwyth University, Aberystwyth SY23 3BZ, UK; o.wyn.roberts@gmail.com, xxl@aber.ac.uk
Received 2014 August 15; accepted 2014 December 25; published 2015 March 13

ABSTRACT

Plasma turbulence at ion kinetic scales in the solar wind is investigated using the multi-point magnetometer data from the Cluster spacecraft. By applying the *k*-filtering method, we are able to estimate the full three-dimensional power spectral density $P(\omega_{sc}, \mathbf{k})$ at a certain spacecraft frequency ω_{sc} in wavevector ($\mathbf{k}$) space. By using the wavevector at the maximum power in $P(\omega_{sc}, \mathbf{k})$ at each sampling frequency ω_{sc} and the Doppler shifted frequency ω_{pla} in the solar wind frame, the dispersion plot $\omega_{pla} = \omega_{pla}(\mathbf{k})$ is found. Previous studies have been limited to very few intervals and have been hampered by large errors, which motivates a statistical study of 52 intervals of solar wind. We find that the turbulence is predominantly highly oblique to the magnetic field $k_\perp \gg k_\parallel$, and propagates slowly in the plasma frame with most points having frequencies smaller than the proton gyrofrequency $\omega_{pla} < \Omega_p$. Weak agreement is found that turbulence at the ion kinetic scales consists of kinetic Alfvén waves and coherent structures advected with plasma bulk velocity plus some minor more compressible components. The results suggest that anti-sunward and sunward propagating magnetic fluctuations are of similar nature in both the fast and slow solar wind at ion kinetic scales. The fast wind has significantly more anti-sunward flux than sunward flux and the slow wind appears to be more balanced.

Key words: solar wind – turbulence – waves

1. INTRODUCTION

Turbulence is an inherently unpredictable process; however, statistical descriptions can be extremely enlightening (Frisch 1995; Tu and Marsch 1995; Bruno & Carbone 2013). The presence of a magnetic field in a plasma causes an anisotropy such that the wavenumber in the perpendicular direction is much larger than that in the parallel direction $k_\perp \gg k_\parallel$ (Shebalin et al. 1983; Goldreich & Sridhar 1995; Matthaeus et al. 1990; Bieber et al. 1996; Horbury et al. 2005; Dasso et al. 2005). At large scales where the magnetohydrodynamic description is applicable the power spectrum follows a Kolmogorov scaling of $-5/3$ comparable to that observed in neutral fluids. At smaller scales a spectral break appears and is followed by a steepening of the power spectra near $k\rho_i \sim 1$ or near $kd_i \sim 1$ (Bourouaine et al. 2012; Bruno & Trenchi 2014), where ρ_i refers to the ion Larmor radius, and d_i refers to the ion inertial length. This may signify the beginning of ion kinetic processes where the magnetohydrodynamic (MHD) description is no longer valid. Typical spectral indices for this range between -3.75 and -1.75 is found at the ion kinetic scales (Alexandrova et al. 2009; Sahraoui et al. 2010b; Alexandrova et al. 2012; Bruno et al. 2014).

The break and the steepening observed in the power spectrum has been interpreted as being due to the damping of kinetic Alfvén waves (Sahraoui et al. 2010b; Podesta 2013) or the dispersion of fast/whistler waves (Biskamp et al. 1996; Li et al. 2001; Stawicki et al. 2001; Gary & Smith 2009), under the hypothesis that the nonlinear nature of turbulence cascade at kinetic scales may be approximated by linear waves. An alternative to the wave interpretation is that these scales are populated by nonlinear coherent structures, such as current sheets or magnetic vortices (Bruno et al. 2003; Osman et al. 2011; Perri et al. 2012; Roberts et al. 2013).

Typically, single spacecraft observations are limited by the inability to differentiate between changes that happen in space and those in time, requiring Taylor's hypothesis to be invoked (Taylor 1938; Perri et al. 2010). This hypothesis may not be valid especially when waves are highly dispersive, flow speed is low ($v_{sw} < v_A$) or when fluctuation amplitudes are large (Klein et al. 2014a; Howes et al. 2014). The four Cluster spacecraft (Escoubet et al. 2001), and their tetrahedral configuration allow spatial and temporal changes to be differentiated fully in three dimensions. One multi-spacecraft method which can be used with Cluster is the *k*-filtering technique (Pinçon & Lefeuvre 1991). Under the assumption that the fluctuations can be described as a superposition of plane waves with random phases, the power spectral density $P(\omega_{sc}, \mathbf{k})$ can then be estimated without the use of Taylor's hypothesis. Recently, the *k*-filtering technique has been further validated for a signal composed of coherent structures (Roberts et al. 2014).

By obtaining the wavevector at the maximum power in the wavevector space at each sampling frequency we can investigate several properties of the fluctuations, such as their directions with respect to the global mean magnetic field $\mathbf{B_0}$, and whether they are directed in the sunward or anti-sunward directions. By Doppler shifting to the plasma frame using

$$\omega_{pla} = \omega_{sc} - \mathbf{k} \cdot \mathbf{V}_{sw}, \quad (1)$$

the dispersion plot of the plasma $\omega = \omega(\mathbf{k})$ can be determined and used as a diagnostic for the plasma waves present.

Constructing a dispersion relation in such a way has been done in several plasma environments (Narita et al. 2004; Tjulin et al. 2008) with the use of the *k*-filtering/wave-telescope technique. This includes several studies in the solar wind (Sahraoui et al. 2010b; Narita et al. 2011b; Roberts et al. 2013; Perschke et al. 2013; Roberts 2014). Unfortunately, the conclusions of these case studies, which all use a small number of time intervals, differ significantly. The results of these studies will be summarized here; Sahraoui et al. (2010b) perform the analysis on an interval of solar wind observing fluctuations that had very low frequencies in the plasma frame, and noted good agreement with the curves obtained from linear Vlasov theory for oblique KAWs. Roberts et al. (2013) also note that these fluctuations may also be explained as being characteristic of populations

Table 1
Table of Plasma and Spacecraft Parameters for Intervals in the Statistical Survey 1 (2004)

	I1	I2	I3	I4	I5
	Jan 19 18:52–19:02 2004	Jan 19 19:02–19:15 2004	Jan 22 01:00–01:10 2004	Jan 22 01:10–01:20 2004	Jan 24 10:25–10:35 2004
$B\,(nT)$	4.4	4.5	5.8	5.3	9.7
$\sigma_{\rm Bdir}$ (°)	18.3	11.2	16.0	20.4	4.8
$\sigma_{\rm Bmag}\,(nT)$	0.49	0.15	0.15	0.18	0.14
$n\,({\rm cm}^{-3})$	3.2	3.3	5.8	5.8	6.6
β	1.93	1.71	1.1	1.3	0.7
$V_{\rm sw}$ (km s^{-1})	602	600	459	478	488
σ_v (km s^{-1})	14	13	13	16	5
f_{ci}Hz	0.067	0.069	0.089	0.081	0.148
v_A km s^{-1}	53.4	54.6	52.8	48.2	82.7
E	0.08	0.09	0.09	0.09	0.05
P	0.03	0.03	0.13	0.13	0.12
θ_{VB}(°)	94.1	94.1	115.0	92.2	82.7
$T_{i\perp}/T_{i\parallel}$	1.61	1.55	1.00	1.17	0.61
ρ_i (km)	223	204	103	118	58
d_i (km)	125	125	94	95	89
n_α/n_p	3.5	3.1	4.2	3.1	0.7

of coherent structures being advected (or moving with a small velocity in the plasma frame) by the plasma bulk velocity, or a combination of both structures and KAW turbulence. Narita et al. (2011b) conclude differently finding little evidence of a linear dispersion relation. Plasma frame frequencies are very high $\omega_p > \Omega_p$ and there is a weak agreement with the curves for fast/whistler waves. The final study performed by Perschke et al. (2013) observed a weak agreement in the dispersion plot for some points with KAWs, ion Bernstein waves at various harmonics of the proton gyrofrequency and some points agreeing with quasi-oblique (60°) fast waves. However, all studies are in agreement that the wavevectors are at highly oblique angles with respect to the global mean field direction, with no quasi parallel fluctuations being observed.

In this paper we perform a statistical study of the dispersion relation in the solar wind magnetic fluctuations. The motivation for this study comes in an attempt to shed some light on the various contradictory results obtained from the four studies reviewed in the previous paragraph. We seek to determine what is the exact nature of these fluctuations and if indeed the dispersion plot is a robust technique to determine the plasma modes present. Two points that were raised in the study of Roberts et al. (2013) is that the errors associated with the velocity measurement are substantial, and that they also may be subject to a systematic error related to differential ion streaming, both can affect the interpretation of results substantially. There are also questions about the validity of using frequency as a diagnostic of the plasma wave, since wave–wave interactions may significantly broaden the frequency (Howes & Nielson 2013). The data selection criteria will be presented in Section 2, followed by presentation of the results, and culminating in a discussion and conclusion.

2. DATA SELECTION

Magnetic field data is obtained from the fluxgate magnetometer (FGM; Balogh et al. 2001) on the Cluster spacecraft (Escoubet et al. 2001). Full resolution data is available with a sampling rate of 22 s^{-1} and spin resolution plasma data (4 s) is available from the Hot Ion Analyzer (HIA) which is one of the two plasma instruments of the Cluster Ion Spectrometer instrument (CIS; Reme et al. 2001). All of the magnetic and plasma data will be taken from C1.

The data intervals studied here are from 2004 and 2005 where the spacecraft had separations of 200 km and 900 km respectively. This allows for the study of the inertial range (data from 2005) and the inertial and dissipation ranges of the solar wind magnetic field turbulence (data from 2004). The intervals include plasmas of various speeds (fast, slow, and possibly disturbed by a coronal mass ejection, CME) and plasma β values in an attempt to give the most comprehensive view of the turbulence irrespective of these values. In total we study 52 intervals; the parameters of these intervals are given in Tables 1–11. In order to obtain as many data sets as possible we have not restricted ourselves to studying one type of wind, and considerations when selecting intervals have been due to spacecraft geometry, and stationarity of the magnetic fields. We have required planarity and elongation to be less than 0.15. In doing so any unphysical results due to an artificial anisotropy caused by under-sampling in one or more directions can be avoided (Sahraoui et al. 2010a).

The magnetic field data is required to be stationary due to a limitation of the method. In this study we require the standard deviation of the magnitude of the magnetic field to be small and that they show no large changes (no discontinuities or shocks). We impose an upper limit for the standard deviation of the magnitude of the magnetic field $\sigma_{\rm Bmag}$ to be less than 0.5nT. This is satisfied for all of the data intervals studied with most intervals being well below this maximum value. The standard deviation of the direction of the magnetic field $\sigma_{\rm Bdir}$ is also required to be less than 20°. Typically the standard deviation on the magnitude is $\sigma_{\rm Bmag} \leqslant 0.2$nT and on the direction $\sigma_{\rm Bdir} \leqslant 10°$.

In order to obtain the Doppler shifted plasma frame frequency $\omega_{\rm pla}$ as accurately as possible, the magnitude of the velocity must also be weakly stationary in a chosen interval. Therefore, we limit ourselves to cases where the standard deviation of the velocity is much smaller than 10% of the velocity measurement, so that the error on the mean velocity is mostly due to the measurement itself rather than temporal changes. This requirement is satisfied well in all intervals, with most standard deviations being $\sigma_v \leqslant 10\,{\rm km\,s^{-1}}$.

Table 2
Table of Plasma and Spacecraft Parameters for Intervals in the Statistical Survey 2 (2004)

	I6	I7	I8	I9	I10
	Jan 24 10:38–10:50 2004	Jan 29 06:30–06:42 2004	Jan 31 14:30–14:40 2004	Jan 31 14:45–14:55 2004	Feb 10 03:20–03:32 2004
$B\,(nT)$	10.1	3.2	8.5	7.9	2.7
$\sigma_{\rm Bdir}\,(^\circ)$	3.7	20.9	12.0	6.8	13.7
$\sigma_{\rm Bmag}\,(nT)$	0.25	0.24	0.20	0.12	0.40
$n\,({\rm cm}^{-3})$	5.5	5.1	3.4	3.3	5.8
β	0.6	4.0	0.62	0.72	2.9
$V_{\rm sw}\,({\rm km\,s}^{-1})$	490	502	613	609	370
$\sigma_v\,({\rm km\,s}^{-1})$	7	9	16	12	5
f_{ci}	0.154	0.049	0.129	0.122	0.042
v_A	93.5	31.1	99.1	96.2	24.9
E	0.07	0.04	0.05	0.04	0.03
P	0.11	0.02	0.07	0.06	0.05
$\theta_{VB}\,(^\circ)$	130.3	73.8	75.1	66.6	79.5
$T_{i\perp}/T_{i\parallel}$	0.59	1.04	1.41	1.28	1.23
ρ_i (km)	57	207	115	121	180
d_i (km)	97	101	122	126	94
n_α/n_p	0.7	3.3	1.6	2.2	NA

Table 3
Table of Plasma and Spacecraft Parameters for Intervals in the Statistical Survey 3 (2004)

	I11	I12	I13	I14	I15
	Feb 10 03:37:30–03:44:00 2004	Feb 10 05:00–05:08 2004	Feb 21 22:40–22:52 2004	Feb 21 23:00–23:15 2004	Feb 21 23:15–23:25 2004
$B\,(nT)$	3.3	3.4	8.9	8.9	8.9
$\sigma_{\rm Bdir}\,(^\circ)$	6.2	6.9	2.5	3.3	5.1
$\sigma_{\rm Bmag}\,(nT)$	0.19	0.10	0.07	0.08	0.09
$n\,({\rm cm}^{-3})$	5.9	5.8	10.2	10.1	10.1
β	2.2	2.3	0.7	0.6	0.6
$V_{\rm sw}\,({\rm km\,s}^{-1})$	365	367	387	384	385
$\sigma_v\,({\rm km\,s}^{-1})$	4	4	3	4	4
$f_{ci}\,(Hz)$	0.050	0.052	0.137	0.136	0.135
$v_A{\rm km\,s}^{-1}$	29.6	30.8	61.1	61.2	61.2
E	0.03	0.08	0.09	0.07	0.07
P	0.04	0.05	0.16	0.14	0.13
$\theta_{VB}(^\circ)$	78.4	66.1	104.7	108.7	110
$T_{i\perp}/T_{i\parallel}$	1.21	0.84	0.77	0.75	0.78
ρ_i (km)	152	131	50	51	51
d_i (km)	94	94	71	72	72
n_α/n_p	NA	0.6	1.6	0.1	1.9

The final criteria for selecting intervals is that the angle between the magnetic field vector and velocity vector $\theta_{\mathbf{vB}} > 60^\circ$ and that the E-field spectrum from the WHISPER instrument is quiet to avoid connection with the foreshock (Etcheto & Faucheux 1984; Lacombe et al. 1985). Any connection to the foreshock may result in backstreaming charged particles (Asbridge et al. 1968; Anderson 1981). Such particles and their associated plasma instabilities are characteristic of the foreshock and not the solar wind which is of interest.

A further step is taken to choose intervals of the free solar wind and not those that are associated with shocks or CMEs. We use the CME catalog of Jian et al. (2006) to check if there are any intervals that may include a CME. We find that some intervals (I3–I6) may be associated with a CME; in the case of I3 and I4 (2004 January 22) the CME arrives at the Active Composition Explorer (ACE) situated at the L1 Lagrange point just after our interval starts and we do not believe that it has any effect on the quality of our data since I4 ends 15 minutes after the CME is detected. The maximum velocity measured at ACE is 700 km s^{-1}. Since L1 is roughly 1.5×10^6 km away, this would give a lead time of roughly 35 minutes, meaning that the arrival time of the CME at Cluster will be well outside the interval (Jian et al. 2006). The other cases are intervals I5–I6 (2004 January 24) with a CME seen to commence at ACE on the 23rd of January and end on the 25th; this appears to be a less powerful CME with a smaller velocity, and, although our interval is in the middle of this time period, density remains low ($<$10 cm^{-3}) within the interval. The results from the analysis are not vastly different from other slow wind intervals. In analyzing solar wind data we must also be aware of Stream Interaction Regions (SIRs) where faster streams collide with slower streams. From a list of SIR events (Jian 2011) it appears that only I7-8 contain SIRs, and the parameters of these intervals are more indicative of fast solar wind. The hourly density and

Table 4
Table of Plasma and Spacecraft Parameters for Intervals in the Statistical Survey 4 (2004)

	I16	I17	I18	I19	I20
	Feb 22 02:20–02:30 2004	Feb 22 02:30–02:40 2004	Feb 24 11:36–11:44 2004	Feb 24 12:20–12:32 2004	Feb 26 18:00–18:08 2004
$B\,(nT)$	8.5	9.2	5.2	5.6	2.5
$\sigma_{\rm Bdir}$ (°)	9.6	3.9	4.4	8.7	8.5
$\sigma_{\rm Bmag}\,(nT)$	0.25	0.13	0.09	0.14	0.08
$n\,({\rm cm}^{-3})$	12.5	11.4	7.3	7.2	21.4
β	0.9	0.6	1.1	0.83	5.3
$V_{\rm sw}$ (km s^{-1})	399	401	396	408	312
σ_v (km s^{-1})	8	5	4	5	2
f_{ci} (Hz)	0.130	0.140	0.081	0.085	0.038
v_A (km s^{-1})	52.8	59.3	42.6	45.8	11.8
E	0.07	0.07	0.08	0.13	0.05
P	0.05	0.05	0.06	0.10	0.10
θ_{VB} (°)	63.3	60.1	93.9	71.7	79.9
$T_{i\perp}/T_{i\parallel}$	0.73	0.89	1.34	1.34	1.19
ρ_i (km)	52	49	100	90	124
d_i (km)	64	67	84	85	49
n_α/n_p	3.2	2.9	1.6	2.8	3.1

Table 5
Table of Plasma and Spacecraft Parameters for Intervals in the Statistical Survey 5 (2004)

	I21	I22	I23	I24	I25
	Feb 26 18:40–18:50 2004	Feb 29 04:10–04:20 2004	Feb 29 04:25–04:35 2004	Mar 2 16:00–16:08 2004	Mar 2 16:10–16:19 2004
$B\,(nT)$	2.5	9.6	9.3	4.9	5.2
$\sigma_{\rm Bdir}$ (°)	2.1	5.0	8.1	8.5	8.3
$\sigma_{\rm Bmag}\,(nT)$	0.16	0.17	0.18	0.17	0.15
$n\,({\rm cm}^{-3})$	21.4	2.8	2.7	1.7	1.8
β	5.3	0.7	0.7	0.9	0.8
$V_{\rm sw}$ (km s^{-1})	312	646	657	668	666
σ_v (km s^{-1})	18	13	18	12	14
$f_{ci}\,(Hz)$	0.038	0.142	0.075	0.079	0.079
v_A (km s^{-1})	11.8	123.1	123.4	81.3	85.5
E	0.05	0.01	0.02	0.15	0.16
P	0.10	0.03	0.01	0.12	0.13
θ_{VB} (°)	79.9	78.6	84.1	83.1	79.4
$T_{i\perp}/T_{i\parallel}$	1.19	1.26	1.46	1.42	1.30
ρ_i (km)	124	129	137	193	178
d_i (km)	49	134	138	171	171
n_α/n_p	1.9	0.3	0.2	2.8	2.8

velocity averages obtained from the ACE spacecraft are shown in Figure 1. The vertical lines denote where the intervals studied are located.

As was mentioned previously the data is taken from 2004 and 2005. The inter-spacecraft distances allow us to probe spacecraft frequencies between 0.06–1 Hz in 2004 and 0.06–0.3 Hz in 2005. These limits are chosen for a number of reasons, in 2004 we choose an upper limit of 1 Hz to avoid spurious results from noise, whereas the choice of 0.3 Hz in 2005 is to avoid spatial aliasing. The lower limits are chosen to avoid data points with large uncertainties due to the technique. It should be noted that the exact frequency ranges where we can use k-filtering depend on the solar wind velocity (and the phase velocity of the waves obtained) as well as the minimum inter-spacecraft distance $d_{\rm min}$ (see Equation (2) where $k_{\rm max} = \pi/d_{\rm min}$). Therefore, the above limits should be taken as a rough estimate and the exact limits used depend on the individual interval in question. The key plasma and spacecraft parameters are presented in Tables 1–11.

$$f_{\rm max} = \frac{k_{\rm max}(V_{\rm sw} - v_{\rm ph})}{2\pi}\cos\theta_{\mathbf{kV}_{\rm sw}}. \quad (2)$$

3. RESULTS

In Figure 2 we show a two-dimensional histogram where we plot the propagation angle $\theta_{\mathbf{kB}_0}$ between the wavevector $\mathbf{k}$ and the global mean magnetic field in the interval $\mathbf{B_0}$. We see that the vast majority of points have highly oblique propagation angles (Sahraoui et al. 2010b; Narita et al. 2011b; Roberts et al. 2013; Perschke et al. 2013) with an average of 88.°6 and a standard deviation of 12.°3. We note that there is a small population of quasi-parallel fluctuations at low frequency, and wavenumber, which could be due to ion cyclotron waves (Jian et al. 2009, 2010). Such quasi-parallel propagating fluctuations

Table 6
Table of Plasma and Spacecraft Parameters for Intervals in the Statistical Survey 6 (2004)

	I26	I27	I28	I29	I30
	Mar 5 00:27–00:36 2004	Mar 5 00:41–00:50 2004	Mar 5 00:51–01:00 2004	Mar 7 07:19–07:28 2004	Mar 7 07:10–07:18 2004
$B\,(nT)$	3.6	3.9	4.1	4.3	4.4
$\sigma_{\rm Bdir}\,(^\circ)$	4.6	2.4	3.4	3.5	11
$\sigma_{\rm Bmag}\,(nT)$	0.26	0.12	0.07	0.08	0.07
$n\,({\rm cm}^{-3})$	4.1	4.2	4.1	6.2	6.8
β	1.6	0.9	0.8	1.3	1.2
$V_{\rm sw}\,({\rm km\,s}^{-1})$	461	466	464	342	345
$\sigma_v\,({\rm km\,s}^{-1})$	6	7	5	3	6
$f_{ci}\,({\rm Hz})$	0.048	0.059	0.061	0.065	0.066
$v_A\,({\rm km\,s}^{-1})$	34.2	41.2	42.7	37.6	36.4
E	0.11	0.12	0.13	0.01	0.01
P	0.09	0.10	0.11	0.04	0.05
$\theta_{VB}\,(^\circ)$	85.6	94.1	91.7	66.6	71.2
$T_{i\perp}/T_{i\parallel}$	1.74	2.21	2.14	0.66	0.76
$\rho_i\,({\rm km})$	189	156	143	83	84
$d_i\,({\rm km})$	112	110	109	91	87
n_α/n_p	0.3	1.7	1.1	1.1	2.1

Table 7
Table of Plasma and Spacecraft Parameters for Intervals in the Statistical Survey 7 (2004)

	I31	I32	I33	I34	I35
	Mar 23 21:22–21:33 2004	Apr 12 00:00–00:06 2004	Apr 12 00:08–00:18 2004	Apr 12 00:20–00:28 2004	Apr 12 00:30–00:38 2004
$B\,(nT)$	4.3	4.3	3.7	4.2	3.9
$\sigma_{\rm Bdir}\,(^\circ)$	12.5	1.8	4.2	4.6	3.4
$\sigma_{\rm Bmag}\,(nT)$	0.08	0.15	0.16	0.16	0.36
$n({\rm cm}^{-3})$	5.5	2.6	2.9	2.5	2.7
β	0.9	0.8	1.2	0.9	1.1
$V_{\rm sw}\,({\rm km\,s}^{-1})$	378	452	453	454	461
$\sigma_v\,({\rm km\,s}^{-1})$	7	33	30	7	9
$f_{ci}\,({\rm Hz})$	0.065	0.065	0.056	0.065	0.058
$v_A\,({\rm km\,s}^{-1})$	39.8	57.3	47.5	58.6	50.7
E	0.05	0.02	0.01	0.01	0.02
P	0.13	0.01	0.02	0.04	0.05
$\theta_{\mathbf{vB_0}}\,(^\circ)$	78.1	78.2	87.5	81.0	74.8
$T_{i\perp}/T_{i\parallel}$	1.06	1.75	1.66	1.63	1.66
$\rho_i\,({\rm km})$	95	160	190	174	188
$d_i\,({\rm km})$	97	139	133	142	137
n_α/n_p	2.1	3.5	0.7	2.9	0.8

have also been observed in measurements of magnetic helicity (He et al. 2011; Podesta & Gary 2011) and the power of such fluctuations was very small or difficult to determine (He et al. 2012; Klein et al. 2014b). The parallel fluctuations are rarely observed using this method, and only occur in 4 of the 52 intervals studied here. A further discussion of these points will be provided elsewhere (in the companion paper this issue, and Roberts 2015). If we omit these fluctuations the mean angle obtained climbs to $90.^\circ1$ and the standard deviation decreases to $7.^\circ8$. The two-dimensional histograms in Figure 2 were obtained with the angle results being placed in bins of 0.02 Hz on the horizontal axis (or $(kv_A/\Omega_p) = 0.02$) and 3° on the vertical axis.

By applying the Doppler shift in Equation (1) to the wavevector obtained at the maximum power $P(\omega_{sc}, \mathbf{k})$, and using the velocity measurement from the CIS instrument we can construct a dispersion plot $\omega_{\rm pla} = \omega_{\rm pla}(\mathbf{k})$. Figure 3 shows a two-dimensional histogram of the dispersion plots covering all 52 intervals studied; in this plot, counts are deposited in bins of size 0.06×0.06. The grey parts of the plot represent no counts, bluer areas have fewer counts and redder areas have more counts. The contour plots overlaid show regions which have 15%, 25%, 50%, 75% of the maximum counts in a single box. The vast majority of points lie between the limits $-0.5 \leqslant \omega_{\rm pla}/\Omega_p \leqslant 0.5$ with a very small proportion above the proton gyrofrequency $\omega_{\rm pla}/\Omega_p > 1$.

The area that has the highest counts is at small frequencies and wavenumbers. This is a result of combining data sets from 2004 and 2005. In this region (between 0–0.3 Hz in the spacecraft frame) we roughly have twice as many samples. The main result here is that the majority of counts are close to zero frequency in agreement with Sahraoui et al. (2010b) and Roberts et al. (2013). However, even this statistical study cannot distinguish between KAWs and coherent structures. It is also difficult

Table 8
Table of Plasma and Spacecraft Parameters for Intervals in the Statistical Survey 8 (2004)

	I36	I37	I38	I39
	Apr 26 06:02:30–06:18:30 2004	Apr 26 06:32–06:44 2004	Apr 26 06:45:00–06:55:30 2004	Apr 26 07:10–07:25 2004
$B\,(nT)$	4.6	4.6	4.6	4.4
$\sigma_{\rm Bdir}$ (°)	6.1	3.8	4.1	4.0
$\sigma_{\rm Bmag}\,(nT)$	0.08	0.09	0.08	0.10
$n\,({\rm cm}^{-3})$	2.2	2.2	2.2	2.3
β	0.95	1.00	0.88	0.98
$V_{\rm sw}$ (km s^1)	496	494	495	489
σ_v (km s^{-1})	11	10	11	10
f_{ci} (Hz)	0.071	0.071	0.071	0.068
v_A (km s^{-1})	68.4	67.8	68.3	64.9
E	0.02	0.01	0.01	0.03
P	0.02	0.02	0.04	0.06
$\theta_{\mathbf{vB_0}}$ (°)	61.1	60.4	61.8	61.9
$T_{i\perp}/T_{i\parallel}$	1.18	1.20	1.30	1.30
ρ_i (km)	163	167	166	174
d_i (km)	152	151	154	151
n_α/n_p	NA	NA	NA	NA

Note. Alpha particle data is unavailable for these intervals. Data from the Active Composition Explorer (ACE) suggests that this very small ($\leqslant$0.5%) in all intervals.

Table 9
Table of Plasma and Spacecraft Parameters for Intervals in the Statistical Survey 9 (2005)

	I40	I41	I42	I43	I44
	Jan 14 15:36–15:44 2005	Jan 14 17:18–17:30 2005	Jan 26 11:03–11:15 2005	Feb 12 02:37–02:50 2005	Feb 16 21:32–21:52 2005
$B\,(nT)$	4.7	5.8	3.1	3.2	11.9
$\sigma_{\rm Bdir}$ (°)	4.5	5.7	7.8	15.5	3.7
$\sigma_{\rm Bmag}\,(nT)$	0.21	0.23	0.20	0.34	0.13
$n\,({\rm cm}^{-3})$	3.9	4.0	4.8	2.3	9.3
β	1.36	0.84	1.51	2.08	0.52
$V_{\rm sw}$ (km s^{-1})	544	547	376	563	367
σ_v (km s^{-1})	7	8	5	13	4
f_{ci} (Hz)	0.071	0.088	0.047	0.048	0.181
v_A (km s^{-1})	51.8	63.4	31.1	45.5	85.2
E	0.005	0.15	0.10	0.11	0.06
P	0.08	0.04	0.12	0.12	0.12
$\theta_{\mathbf{vB_0}}$ (°)	101.8	82.5	91.6	85.4	118.0
$T_{i\perp}/T_{i\parallel}$	1.68	1.95	1.42	2.19	0.46
ρ_i (km)	175	146	154	319	37
d_i (km)	115	114	105	149	75
n_α/n_p	1.8	2.6	3.8	0.6	5.6

to determine whether waves at low wavenumbers are propagating in the sunward or the anti-sunward direction. The region where the highest counts occur in Figure 3 may be described by KAWs, or structures (Sahraoui et al. 2010b; Roberts et al. 2013), but not whistler waves, which if present would be a minority component at these scales. It is also known that quasi-perpendicularly propagating kinetic slow waves have similar frequencies to the KAWs and such waves have a contribution especially to the compressible wave power (Howes et al. 2012).

The statistical study presented in the current section is the combination of heterogeneous intervals with a wide variety of plasma parameters. Any subtle characteristics of a small number of intervals will have small significance with the properties seen in the majority of intervals dominating. It is well known that the fast and slow solar wind has different characteristics in terms of their heating mechanisms and the behavior of the embedded waves/turbulence (Tu & Marsch 1991; Leamon et al. 1998; Hamilton et al. 2008; Bruno & Carbone 2013). Now we will analyze fast and slow wind intervals separately to see if we can find any significant differences. The angle plots for the two types of wind are not reproduced as there is no significant difference, with both wind types giving $\theta_{\mathbf{kB_0}} \sim 90^\circ$.

We define fast wind intervals to be when the solar wind velocity $V_{\rm sw} > 540\,{\rm km\,s^{-1}}$.[1] Four of these intervals were analyzed in the case study presented in Roberts et al. (2013). We then define intervals that have speeds $V_{\rm sw} < 450\,{\rm km\,s^{-1}}$ to be slow wind. However, this leaves many intervals in the intermediate range. To determine whether these should be

[1] This includes intervals I1, I2, I8, I9, I22, I23, I24, I25, I40, I41, I43.

Table 10
Table of Plasma and Spacecraft Parameters for Intervals in the Statistical Survey 10 (2005)

	I45	I46	I47	I48	I49
	Feb 16 22:10–22:24 2005	Feb 16 22:24–22:40 2005	Feb 19 06:04–06:20 2005	Feb 19 06:20–06:34 2005	Feb 19 06:34–06:50 2005
$B\,(nT)$	11.9	11.9	5.8	6.4	6.2
$\sigma_{\rm Bdir}$ (°)	2.5	2.8	11.6	4.4	2.2
$\sigma_{\rm Bmag}\,(nT)$	0.12	0.08	0.17	0.3	0.4
$n\,({\rm cm}^{-3})$	9.2	9.1	9.8	8.6	8.5
β	0.50	0.51	0.89	0.63	0.66
$V_{\rm sw}$ (km s^{-1})	377	376	501	500	498
σ_v (km s^{-1})	4	4	5	10	12
f_{ci} (Hz)	0.181	0.181	0.089	0.098	0.094
v_A (km s^{-1})	85.8	85.8	40.8	47.7	46.5
E	0.02	0.03	0.10	0.09	0.07
P	0.13	0.14	0.12	0.12	0.12
$\theta_{\mathbf{vB_0}}$ (°)	109.4	112.0	89.6	83.0	82.0
$T_{i\perp}/T_{i\parallel}$	0.51	0.48	2.36	2.55	2.64
ρ_i (km)	38	38	106	98	104
d_i (km)	75	75	73	77	78
n_α/n_p	0.8	1.3	3.5	3.7	1.9

Table 11
Table of Plasma and Spacecraft Parameters for Intervals in the Statistical Survey 11 (2005)

	I50	I51	I52
	Feb 21 16:10–16:22 2005	Feb 21 16:23–16:36 2005	Feb 21 17:38–17:50 2005
$B\,(nT)$	5.4	5.3	4.5
$\sigma_{\rm Bdir}$ (°)	3.1	1.9	3.6
$\sigma_{\rm Bmag}\,(nT)$	0.07	0.09	0.17
$n\,({\rm cm}^{-3})$	3.1	3.0	4.0
β	0.51	0.59	1.05
$V_{\rm sw}$ (km s^{-1})	401	404	398
σ_v (km s^{-1})	8	7	7
f_{ci} (Hz)	0.083	0.081	0.069
v_A (km s^{-1})	68.1	66.4	49.4
E	0.03	0.01	0.11
P	0.13	0.14	0.11
$\theta_{\mathbf{vB_0}}$ (°)	110.4	112.6	115.6
$T_{i\perp}/T_{i\parallel}$	1.36	1.25	1.09
ρ_i (km)	109	112	122
d_i (km)	130	130	113
n_α/n_p	1.1	2.4	2.6

considered in our analysis of the slow wind, we consider speeds in the interval $450 > v_{\rm sw} > 500\,{\rm km\,s^{-1}}$ which satisfy the density criteria $n > 4{\rm cm}^{-3}$ in our slow wind analysis. Intervals that do not fall into these criteria are eliminated from further analysis. In total, we study 11 intervals of fast solar wind and 30 intervals of slow solar wind while 11 are eliminated. The two-dimensional histogram showing the dispersion plot of the fast (and slow) wind cases is shown on the left (right) in Figure 4. The two plots are quite similar. At low wavenumbers magnetic field fluctuations are close to $\omega_{\rm pla} \sim 0$, and there is a large spread of values with both positive and negative frequencies. However, there does seem to be a small increase in frequency as the wavenumber kv_A/Ω_p rises between 0.6–1.3, where an enhanced area of counts curves up. This agrees with the dispersion of kinetic Alfvén waves with near perpendicular propagation angles according to linear Vlasov theory (see the dispersion curves in Figure 3). A marked difference between the fast and slow wind dispersion plots is that the Doppler shifted frequency $\omega_{\rm pla}/\Omega_p$ has a substantially wider spread of values in the slow wind than in the fast wind. Another difference is that while the fast wind has more data points where $\omega_{\rm pla}/\Omega_p$ is positive, the slow wind appears to be more evenly distributed at positive and negative values. This may suggest that in the fast wind, there are more magnetic fluctuations propagating in the anti-sunward direction than in the sunward direction. In the slow wind, the fluctuations propagating in the two directions are more balanced. Later on, we will see that the power of anti-sunward and sunward fluctuations have similar behavior. However, since we have fewer fast wind cases, it is difficult to point out any differences definitively.

In Figure 4, linear least squares fitting for the positive and negative frequencies is shown as dashed lines. The gradients of the linear least squares fitting for the positive and negative frequencies shown in Figure 4 have similar absolute values for both the fast and slow solar wind. This may suggest that the anti-sunward and sunward magnetic field fluctuations have similar dispersion relations.

A relevant issue pointed out by Roberts et al. (2013) is that the presence of alpha particles, and other heavier ions can affect the measurement of the proton bulk velocity $V_{\rm sw}$ since the ion bulk velocity V_f measured by CIS is based on the assumption that all recorded ions are protons. $V_{\rm sw}$ is used to Doppler shift the spacecraft frequency ω_{sc} to the plasma frame frequency $\omega_{\rm pla}$ (see Equation (1)). A substantial presence of alpha particles may affect the accuracy of V_f and consequently the accuracy of $\omega_{\rm pla}$ especially at large k. The correction suggested by Roberts et al. (2013) is given as

$$V_{\rm sw} = \sqrt{\frac{1+\frac{n_\alpha}{n_p}}{1+\frac{2n_\alpha}{n_p}}}\,V_f. \qquad (3)$$

The correction will be larger for higher alpha particle abundances, higher measured velocities V_f, and will have more effect at larger wavenumbers. In extreme cases when we have both large velocities and alpha particle abundance this systematic error can be as large as $\pm\Omega_p$ at large wavenumbers (Roberts 2014).

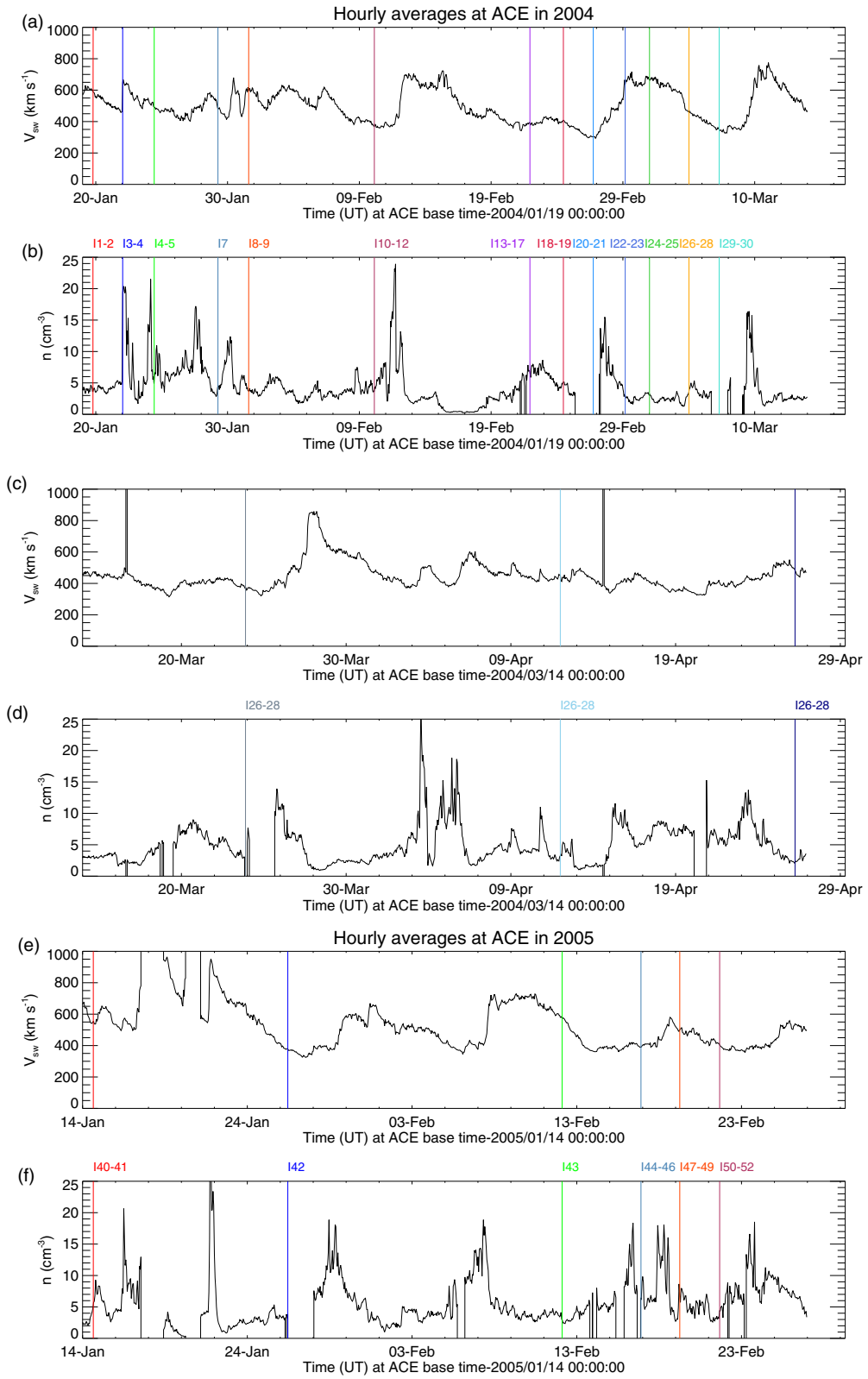

Figure 1. Panels (a), (c), and (e) show the hourly averages of the radial velocity of the solar wind at the L1 Lagrange point measured by ACE in 2004 (a and c) and 2005 (e). Panels (b), (d), and (f) show the corresponding hourly averages of number density of protons. Missing data are denoted by large positive (velocity) and negative (density) values and lie out of the plotting range

Figures 5(a) and (b) shows the number of counts for the positive and negative frequencies as a function of wavenumber with (without) the alpha particle correction suggested by Roberts et al. (2013). Here we assume that negative frequencies are sunward propagating waves. In Figures 5(a) and (b), the red curves show the proportion of the anti-sunward waves. It can be seen that the correction significantly modifies the number of sunward waves. The proportion of anti-sunward waves climbs from a mean value of around 50% to around 60%. This may also be an underestimation, since several measured

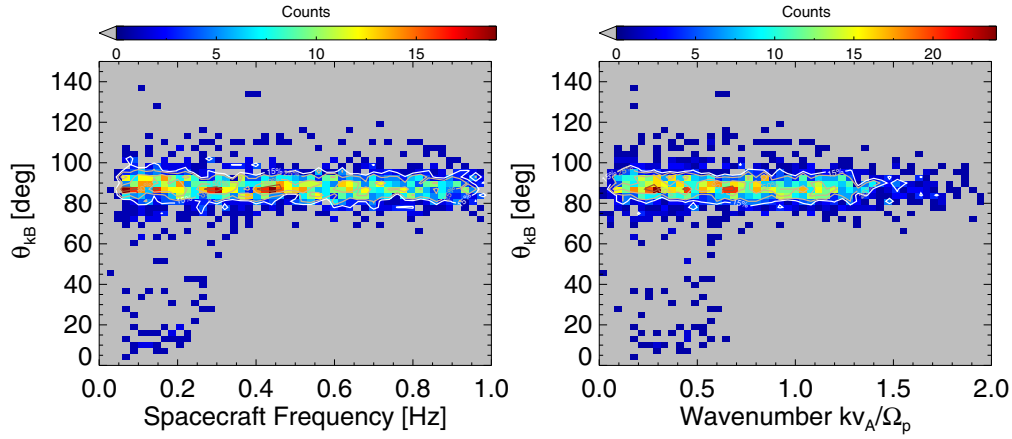

Figure 2. Plots of the angle that the wavevector at the maximum value of $P(\omega, \mathbf{k})$ makes with the global mean magnetic field $\mathbf{B_0}$ as a function of spacecraft frequency (left) and wavenumber (right). The contours denote to 15% (dark brown), 25% (light brown), 50% (white), and 75% (dark red) of the maximum counts. The coding of contours will be the same in all of the figures.

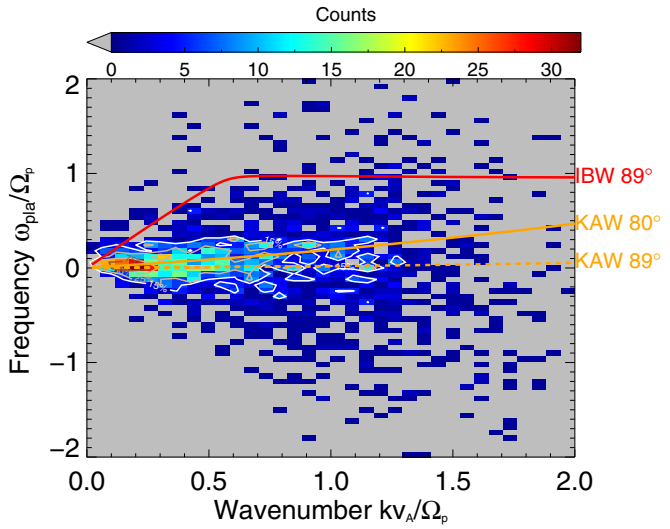

Figure 3. Two-dimensional histogram with the dispersion points from all 52 intervals with curves from linear Vlasov solver of Li & Habbal (2001) for ion Bernstein at $\theta_{\mathbf{kB}} = 89°$ and kinetic Alfvén waves at $\theta_{\mathbf{kB}} = 80°$ and 89°.

negative frequencies might in fact be positive within the limit of uncertainties (Roberts et al. 2013). We remark that this is an important issue when considering the sunward/anti-sunward interpretation of waves, and simply taking the absolute value of the frequency may be misleading given the systematic error due to alpha particles and other errors such as from the bulk velocity measurement.

The dispersion plot including all the 52 intervals is given in Figure 5(c) and (5(d)) without (with) the correction due to the presence of alpha particles. The overall difference with and without the correction is small with intervals chosen mainly because the abundance of alpha particles is less than 3%. However, the difference in the gradients of the two linear least squares fits of the data shows that the difference can affect the interpretation of the results. For case studies especially, when we have fewer intervals the effect of the correction may be more pronounced.

After applying this correction we investigate the anti-sunward and the sunward powers by considering the ratio, $(P_{\rm out} - P_{\rm in})/(P_{\rm out} + P_{\rm in})$, which will give a value of 1 if all the power is in the anti-sunward direction and -1 if the power is in the sunward direction. Here $P_{\rm in}$ and $P_{\rm out}$ represent the average value of the combined normalized (to B_0^2 for each interval) power of sunward and anti-sunward propagating fluctuations. The result shown in Figure 6. The ratio $(P_{\rm out} - P_{\rm in})/(P_{\rm out} + P_{\rm in})$ is plotted in Figure 6(a) and 6(b) for the fast (slow) wind as a function of the wavenumber bin k. The averaged power is given in Figure 6(c) and 6(d) for the fast and slow wind, respectively. The orange dashed lines denote the weighted averages of the power ratio

$$P_r = \frac{\Sigma_{k=1}^{n}\left(P_k \sigma_k^{-2}\right)}{\Sigma_{k=1}^{n}\sigma_k^{-2}} \quad (4)$$

where P_k is the power ratio at a given wavenumber bin k and σ is the error on that bin. The σ denotes the standard deviation of the powers in the bins normalized to the maximum power in the bin. The larger error bars on the fast solar wind cases shown in Figure 6(a) are due to less counts in each bin, with an average of 20 counts per bin while the slow cases have average of 50 counts per bin.

In the fast solar wind the power is dominantly outward with a weighted average of 0.19, while in the slow solar wind the power is more balanced with a weighted average of -0.06 for the slow wind cases. This suggests that there may be a subtle difference between the fast and the slow solar wind turbulence (Bruno & Carbone 2013).

4. DISCUSSION

In this study we considered a large number of intervals using the k-filtering technique, and found that the turbulence is highly anisotropic with $k_\perp \gg k_\parallel$ at all scales except for in four intervals studied where there exists a small number of points at quasi-parallel propagation $k_\parallel \gg k_\perp$ at low wavenumbers $kv_A/\Omega_p \leqslant 0.6$. The four intervals make up a small fraction of the total data surveyed but may yield some new insights, and will be studied in detail (see the companion paper this issue, Roberts & Li 2015). Turbulence at ion kinetic scales still has more power in the anti-sunward direction in the fast solar wind while more balanced in the slow solar wind. However, conclusions should be tentative since the number of intervals that are suitable for study are limited by the data requirements set out in Section 2 especially for the fast wind.

Analysis of the dispersion plot is hampered by large uncertainties in the velocity measurement, which is the dominant source of error when Doppler shifting the frequency to the

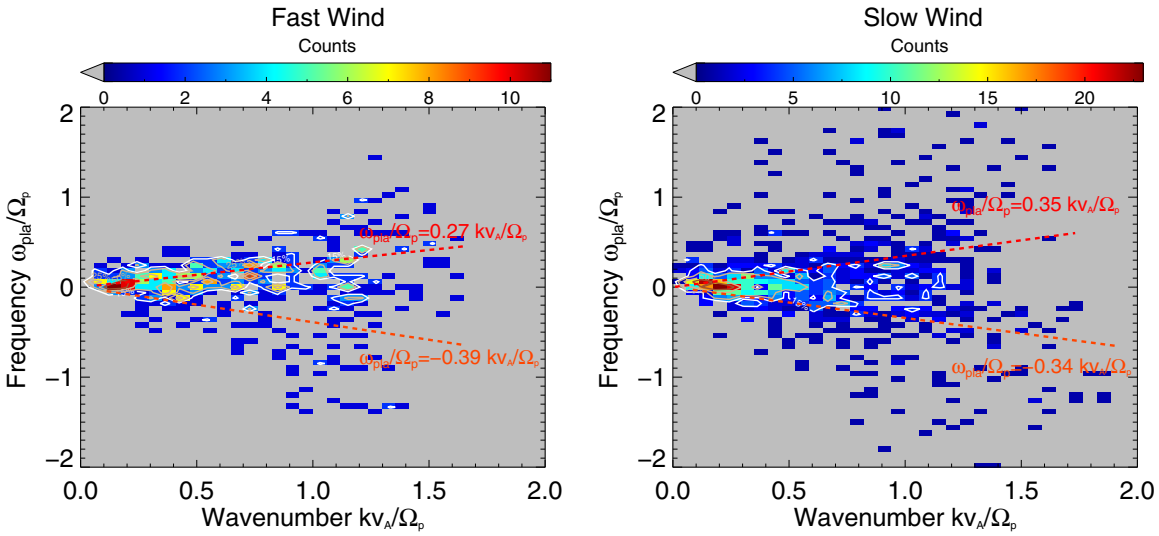

Figure 4. Two dimensional histogram with bins of 0.06 × 0.06 made up of only fast solar wind (11 intervals) cases $V_{sw} > 540\,\mathrm{km\,s^{-1}}$ (left) and only (41 intervals) slow solar wind cases $V_{sw} < 470\,\mathrm{km\,s^{-1}}$. The red (orange) dashed line denotes a linear least squares fitting to the data for positive (negative) points.

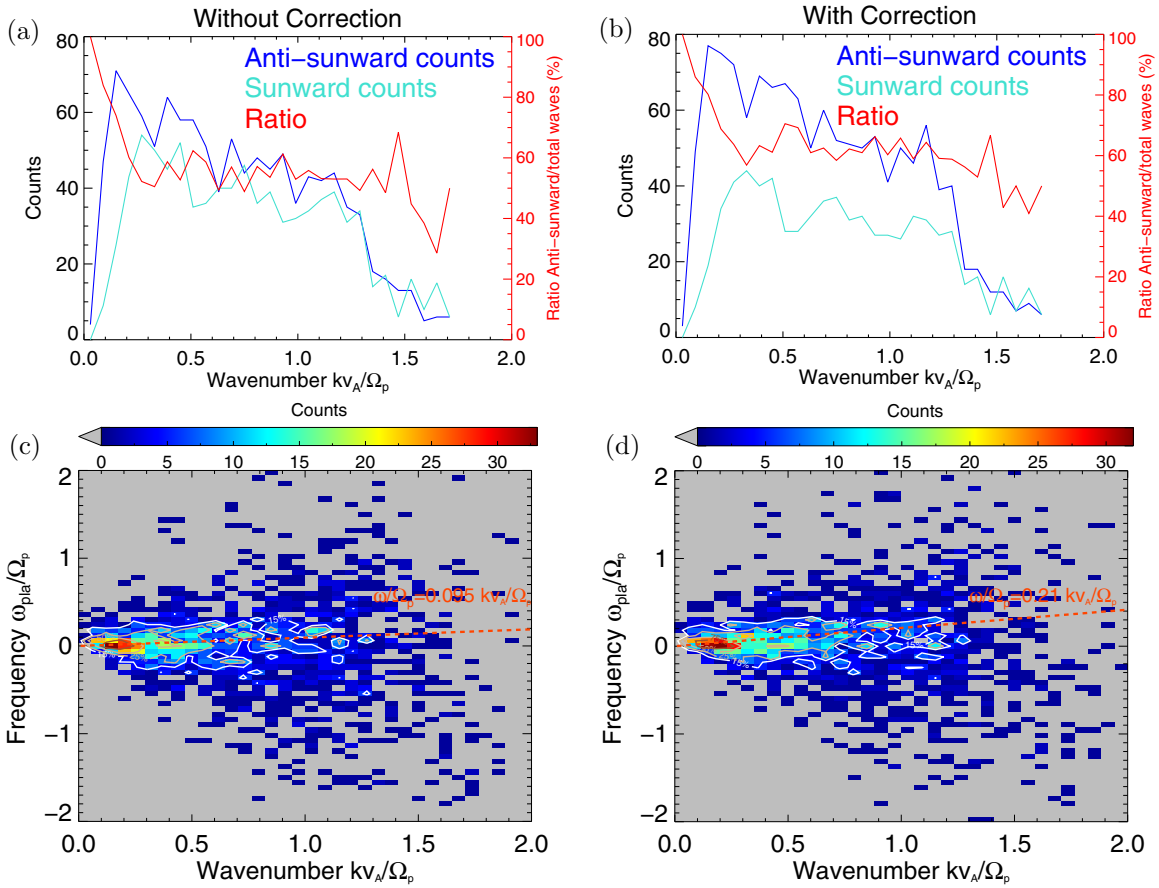

Figure 5. Top row: counts of negative (sunward) and positive (anti-sunward) waves as a function of the wavenumber obtained from *k*-filtering without the correction (a) and with (b). Bottom row: dispersion plots of all intervals without (c) and with (d) the corrections. A linear least squares fitting is shown in the orange dashed lines to quantify the effect of the correction.

plasma frame. The error on the wavevector is small in comparison to the error on the velocity measurement (e.g., Sahraoui et al. 2010a). In this work, we try to improve the investigation of the dispersion relation by having a larger number of time intervals to minimize statistical uncertainties due to the velocity measurement. The dispersion plot shows that most points have frequencies less than the ion gyration frequency $\omega < \Omega_p$ with most counts in the vicinity of $\omega \sim 0$. There are some points at frequencies higher than the proton gyration frequency $\omega > \Omega_p$. However, they make up only a small number of the total data points obtained and are statistically less significant than the points where $\omega < \Omega_p$.

The relative drift of alpha particles can significantly affect the measurement of the proton velocity, introducing a

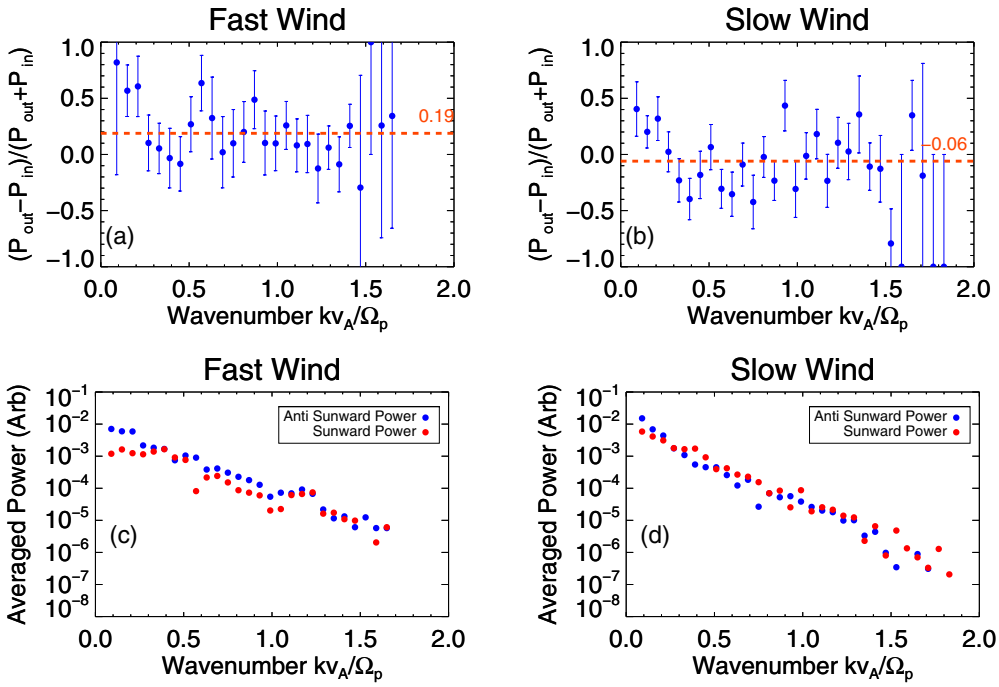

Figure 6. (a and b) shows the ratios of the powers $(P_{\rm out} - P_{\rm in})/(P_{\rm out} + P_{\rm in})$, where +1 denotes all power being anti-sunward and −1 denotes all power being sunward, as a function of wavenumber for fast and slow cases. The orange dashed lines denote the weighted average of $(P_{\rm out} - P_{\rm in})/(P_{\rm out} + P_{\rm in})$. (c) and (d) show the evolution of the total sunward and anti-sunward power as a function of wavenumber bin.

large systematic error on the proton velocity measurement. Many of the intervals studied here have very low alpha particle abundances and the effect is small for most intervals, but a larger alpha particle abundance may make the Doppler shifted frequency in the plasma frame inaccurate if the correction is not performed.

When considering the dispersion plots for fast and slow wind separately we see some subtle differences. In both cases most points are close to $\omega_{\rm pla}/\Omega_p \sim 0$ consistent with either KAW turbulence or coherent structures, or a combination of them (Roberts et al. 2013). For the fast wind the frequency shows a small spread, and increases slightly at larger wavenumbers for both anti-sunward and sunward propagating fluctuations, which is predicted for KAWs. For both the fast and slow wind, the best linear least square fitting to the $\omega_{\rm pla} - k$ relationship shows that the fluctuations have frequencies (magnitude) increasing at larger k and the gradients of the increase for both sunward and anti-sunward fluctuations are similar. This may suggest that anti-sunward and sunward propagating magnetic fluctuations have similar or the same physical nature at the ion kinetic scales studied.

We note that there are still sizable number (although the counts are small) data points that have the frequency spread (up to $|\omega_{\rm pla}|/\Omega_p \sim 2$) in the slow wind. This suggests that turbulence in the slow wind is more compressible than in the fast wind. We cannot rule out possible contributions of plasma waves such as kinetic fast waves. It has also be suggested that wave–wave interactions may be important in broadening the dispersion plot, e.g., (Howes & Nielson 2013). However, the majority of points in this survey of both fast and slow wind are consistent with KAWs and/or coherent structures.

The negative frequencies detected in both the fast and slow solar wind in Figure 4 could be interpreted as waves propagating sunward. By considering the powers of waves traveling in both directions as a function of wavenumber, we see that the domination of anti-sunward waves over sunward waves is progressively weakened at ever smaller scales in the fast solar wind continuing the trend at MHD scales in the fast solar wind (Tu et al. 1990). It is well established that on large scales, anti-sunward propagating Alfvén waves are dominating over sunward propagating waves especially in the fast solar wind (Belcher 1971). The loss of the domination of the anti-sunward waves is largely due to the relative strengthening of the sunward propagating waves at high frequencies/wavenumbers, again similar to the case in the frequency band $10^{-3} \sim 10^{-2}$ Hz observed by Helios (Tu et al. 1990). Here the slow solar wind repeats the same trend although the domination of anti-sunward waves at small wavenumbers is less pronounced than in the fast solar wind.

For both the fast and slow solar wind, the relative weakening of the anti-sunward over sunward waves at small wavenumbers continues until at $kv_A/\Omega_p \sim 0.3$ (slow wind) and 0.35 (fast wind) where the anti-sunward and sunward fluctuations have equal power. The trend continues until $kv_A/\Omega_p \sim 0.4$ (slow wind) and 0.45 (fast wind) after which the trend has a reversal. We speculate that the later numbers may indicate the initiation of ion kinetic processes.

Narita et al. (2011a) find that in the solar wind sunward waves are dominating at $kv_A/\Omega_p \sim 1$ while Perschke et al. (2013) find again that for a fast solar wind sunward waves are dominating at $1.6 \leqslant kv_A/\Omega_p < 3$ (however, due to the magnitude of the solar wind speed and the limit of the k-filtering technique, we are unable to reach k values as large as those in Perschke et al. 2013). Our result is that in the slow wind the power ratio $(P_{\rm out} - P_{\rm in})/(P_{\rm out} + P_{\rm in})$ is close to 0 at ion kinetic scales and the power ratio is close to 0 (sunward and anti-sunward waves are largely balanced) at $1 < kv_A/\Omega_p < 1.6$ appear to be different to the results by (Narita et al. 2011a; Perschke et al. 2013). Their difference could be due to a number of factors: for the intervals studied by Narita et al. (2011a) the craft were

close to the foreshock, and there could be some sunward waves associated with the foreshock produced by backstreaming particles. Secondly, the elongation and planarity of the Cluster spacecraft for the time intervals studied by these studies are $E > 0.3$ and $P > 0.1$, which is much larger than the criteria used in this study, and may be undesirable for applying the k-filtering (Sahraoui et al. 2010a) in such geometries. Thirdly, these studies were based on a small number of intervals. Furthermore, the error bars presented by Perschke et al. (2013) are the variance of the power ratios. The errors on the velocity measurement related to the alpha particles have not been accounted for. The large errors can make it difficult to determine which waves are indeed sunward and which are anti-sunward.

Several mechanisms may contribute to the observed magnetic field fluctuations in Figure 6: MHD waves (mainly Alfvén waves), coherent structures, and waves produced by local plasma instabilities. The MHD waves are mainly propagating in the anti-sunward direction so they may contribute to a large ratio $(P_{\rm out} - P_{\rm in})/(P_{\rm out} + P_{\rm in})$. On the other hand, the distribution of coherent structures at various scales (such as static structures, current sheets, Alfvén vortices, and pressure balanced structures) may be random in space and these structures are expected to produce $(P_{\rm out} - P_{\rm in})/(P_{\rm out} + P_{\rm in}) \approx 0$ on average. It is known that at MHD scales magnetic structures increase between 0.3 AU and 1 AU in the fast solar wind while no such evolution is seen in the slow solar wind (Bruno et al. 2007). Our result may suggest that at ion kinetic scales structures contribute more to the ion kinetic scale turbulence in the slow solar wind than in the fast solar wind. A parametric instability of anti-sunward propagating Alfvén waves may also contribute to the generation of sunward propagating Alfvén waves and anti-sunward propagating sound waves Tu et al. (1989). Such an instability is certainly more likely to contribute to wave generation at very low frequencies where the amplitude of the anti-sunward propagating Alfvén waves is strong. The contribution of such instabilities to the wave generation at ion kinetic scales studied in this work is more difficult but has been discussed in numerical simulations (Matteini et al. 2010; Gao et al. 2014). However, the parametric instability is not expected to account for the observed increase of the power ratio at $1 < kv_A/\Omega_p < 1$ since (anti-sunward) sound waves are subject to Landau damping while the daughter Alfvén waves are subject to less damping in a warm plasma such as the solar wind at 1AU. A cross scale generation mechanism has also been suggested to produce magnetic fluctuations at kinetic scales (Voitenko & Goossens 2005; Zhao et al. 2014). Plasma temperature anisotropy instabilities and stream/stream instabilities may also be able to contribute to the observed increase of $(P_{\rm out} - P_{\rm in})/(P_{\rm out} + P_{\rm in})$ at $0.5 \leqslant kv_A/\Omega_p < 1.1$.

We conjecture that due to the existence of a proton beam component and the fact that alpha particles often flow faster, protons may favor the production of waves propagating in the anti-sunward direction at ion scales. With these assumptions, we can tentatively explain the results of $(P_{\rm out} - P_{\rm in})/(P_{\rm out} + P_{\rm in})$ in Figure 6 for both the fast and slow wind. However, it is important to note that the powers used here are the powers associated with a maximum. In reality there is a plane of solutions in wave space that separate sunward and anti-sunward waves. A more in-depth study would look at the integrated power on either side of this plane.

Finally, we note that a new decrease of $(P_{\rm out} - P_{\rm in})/(P_{\rm out} + P_{\rm in})$ roughly occurs at $kv_A/\Omega_p > 1$. We notice that instabilities such as plasma temperature anisotropy instabilities and stream/stream instabilities often have a upper limit at around $kv_A/\Omega_p \sim 1$. However, we have practiced caution here since at larger k, errors are large.

5. CONCLUSIONS

To conclude, we have presented a statistical study using the k-filtering technique for the fast and the slow solar wind. It is found that at ion kinetic scales ($0.1 < kv_A/\Omega_p < 1.6$) the frequencies of magnetic field fluctuations are mostly at low frequencies in the plasma frame consistent with the interpretation presented in Roberts et al. (2013). Our results suggest that statistically speaking, the dispersion relation plots show that in both the fast and slow solar wind, anti-sunward and sunward propagating fluctuations are of similar nature and they are consistent to the picture that KAWs and coherent structures are populated in the ion kinetic scales. In the fast wind, the spread of $\omega_{\rm pla}/\Omega_p$ is small while in the slow wind the frequencies are found to be broadened much more. We suggest that the slow solar wind is in a more developed state of turbulence. Our results are consistent with the scenario that the slow solar wind contains more structures, which may correspond to its origin on closed magnetic field lines on the Sun. The fast wind was shown to have significantly more anti-sunward flux than sunward flux and the slow wind appears to be more balanced. Finally, the angle plots revealed some quasi parallel fluctuations, which will be investigated in more detail in a separate study (Roberts & Li 2015).

All Cluster data are obtained from the ESA Cluster Active Archive. We thank the FGM and CIS instrument teams and the ESA Cluster Active Archive.

REFERENCES

Alexandrova, O., Lacombe, C., Mangeney, A., Grappin, R., & Maksimovic, M. 2012, ApJ, 760, 121
Alexandrova, O., Saur, J., Lacombe, C., et al. 2009, PhRvL, 103, 165003
Anderson, K. 1981, JGR, 86, 4445
Asbridge, J., Bame, S., & Strong, I. 1968, JGR, 73, 5777
Balogh, A., Carr, C. M., Acuna, M. H., et al. 2001, AnGeo, 19, 1207
Belcher, J. W. 1971, ApJ, 168, 509
Bieber, J., Wanner, W., & Matthaeus, W. 1996, JGR, 101, 2511
Biskamp, D., Schwarz, E., & Drake, J. F. 1996, PhRvL, 76, 1264
Bourouaine, S., Alexandrova, O., Marsch, E., & Maksimovic, M. 2012, ApJ, 749, 102
Bruno, R., & Carbone, V. 2013, LRSP, 10, 2
Bruno, R., Carbone, V., Sorriso-Valvo, L., & Bavassano, B. 2003, JGR, 108, SSH 8
Bruno, R., DAmicis, R., Bavassano, B., Carbone, V., & Sorriso-Valvo, L. 2007, AnGeo, 25, 1913
Bruno, R., & Trenchi, L. 2014, ApJL, 787, L24
Bruno, R., Trenchi, L., & Telloni, E. 2014, ApJL, 793, L15
Dasso, S., Milano, L., Matthaeus, W., & Smith, C. 2005, ApJ, 635, 181
Escoubet, C., Fehringer, M., & Goldstein, M. 2001, AnGeo, 19, 1197
Etcheto, J., & Faucheux, M. 1984, JGR, 89, 6631
Frisch, U. 1995, Turbulence: The Legacy of A. N. Kolmogorov (Cambridge: Cambridge Univ. Press)
Gao, X., Lu, Q., Li, X., et al. 2014, ApJ, 780, 56
Gary, S. P., & Smith, C. W. 2009, JGR, 114, A12105
Goldreich, P., & Sridhar, S. 1995, ApJ, 438, 763
Hamilton, K., Smith, C. W., Vasquez, B. J., & Leamon, R. J. 2008, JGRA, 113, 1106
He, J., Marsch, E., Tu, C.-Y., Yao, S., & Tian, H. 2011, ApJ, 731, 85
He, J., Tu, C., Marsch, E., & Yao, S. 2012, ApJ, 749, 86
Horbury, T., Forman, M. A., & Oughton, S. 2005, PPCH, 47, B703
Howes, G., Klein, K. G., & TenBarge, J. M. 2014, ApJ, 789, 106
Howes, G., & Nielson, K. D. 2013, PhPl, 20, 072302
Howes, G. G., Bale, S. D., Klein, K. G., et al. 2012, ApJL, 753, L19

Jian, L., Russell, C. T., Luhmann, J. G., & Skoug, R. M. 2006, SoPh, 239, 393
Jian, L. K., Russell, C. T., Luhmann, J. G., et al. 2009, ApJL, 701, L105
Jian, L. K., Russell, C. T., Luhmann, J. G., et al. 2010, JGR, 115, A12
Jian, L. K., Russell, C. T., & Luhmann, J. G. 2011, SoPh, 274, 321
Klein, K., Howes, G., & TenBarge, J. M. 2014a, ApJL, 789, L20
Klein, K. G., Howes, G. G., TenBarge, J. M., & Podesta, J. J. 2014b, ApJ, 785, 138
Lacombe, C., Mangeney, A., & Harvey, CC. 1985, JGR, 90, 73
Leamon, R. J., Smith, C. W., Ness, N. F., Matthaeus, W. H., & Wong, H. 1998, JGR, 103, 4775
Li, H., Gary, S. P., & Stawicki, O. 2001, GeoRL, 28, 1347
Li, X., & Habbal, S. 2001, JGR, 106, 10669
Matteini, L., Landi, S., Velli, M., & Hellinger, P. 2010, JGRA, 115, 9106
Matthaeus, W., Goldstein, M., & Roberts, D. A. 1990, JGR, 95, 20673
Narita, Y., Gary, S. P., Saito, S., Glassmeier, K., & Motschmann, U. 2011a, GeoRL, 38, L5101
Narita, Y., Glassmeier, K., Goldstein, M., Motschmann, U., & Sahraoui, F. 2011b, AnGeo, 29, 1731
Narita, Y., Glassmeier, K., Schäfer, S., et al. 2004, AnGeo, 22, 2315
Osman, K., Matthaeus, W., Greco, A., & Servidio, S. 2011, ApJL, 727, L11
Perri, S., Carbone, V., & Veltri, P. 2010, ApJL, 725, L52
Perri, S., Goldstein, M., Dorelli, J., & Sahraoui, F. 2012, PhRvL, 109, 191101
Perschke, C., Narita, Y., Gary, S. P., Motschmann, U., & Glassmeier, K.-H. 2013, AnGeo, 31, 1949
Pinçon, J., & Lefeuvre, F. 1991, JGR, 96, 1789
Podesta, J. 2013, SoPh, 286, 529
Podesta, J. J., & Gary, S. P. 2011, ApJ, 734, 15
Reme, H., Aoustin, C., Bosqued, J. M., et al. 2001, AnGeo, 19, 1303
Roberts, O. W. 2014, PhD thesis, Aberystwyth Univ.
Roberts, O. W., & Li, X. 2015, ApJ, 802, 1
Roberts, O. W., Li, X., & Jeska, L. 2014, GID, 3, 247
Roberts, O. W., Li, X., & Li, B. 2013, ApJ, 769, 58
Sahraoui, F., Belmont, G., Goldstein, M., & Rezeau, L. 2010a, JGR, 115, 1
Sahraoui, F., Goldstein, M., Belmont, G., Canu, P., & Rezeau, L. 2010b, PhRvL, 105, 131101
Shebalin, J., Matthaeus, W., & Montgomery, D. 1983, JPlPh, 29, 525
Stawicki, O., Gary, S. P., & Li, H. 2001, JGR, 106, 8273
Taylor, G. I. 1938, RSPSA, 164, 476
Tjulin, A., Lucek, E. A., & Dandouras, I. 2008, JGR, 113, A08113
Tu, C.-Y., & Marsch, E. 1991, AnGeo, 9, 319
Tu, C.-Y., & Marsch, E. 1995, SSRv, 73, 1
Tu, C., Marsch, E., & Rosenbauer, H. 1990, GeoRL, 17, 283
Tu, C. Y., Marsch, E., & Thieme, K. M. 1989, JGR, 94, 11739
Voitenko, Y., & Goossens, M. 2005, PhRvL, 94, 135003
Zhao, J. S., Voitenko, Y., Wu, D. J., & De Keyser, J. 2014, ApJ, 785, 139